LA-UR-01-2682
Approved for public release;
distribution is unlimited.

Title: **Velocity-Field measurements of a shock-accelerated fluid instability**

Author(s): Katherine Prestridge, Cindy A. Zoldi, Peter Vorobieff, Paul M. Rightley and Robert F. Benjamin

Submitted to:

http://lib-www.lanl.gov/la-pubs/00796096.pdf

Velocity-field measurements of a shock-accelerated fluid instability

Katherine Prestridge[1], Cindy A. Zoldi[1], Peter Vorobieff[2], Paul M. Rightley[1], and Robert F. Benjamin[1]

[1] Los Alamos National Lab, Los Alamos NM 87545, USA
[2] University of New Mexico, Albuquerque NM 87131, USA

Abstract. A cylinder of heavy gas (SF_6) in air is hit by a Mach 1.2 shock. The resultant Richtmyer-Meshkov instability is observed as it propagates through the test section of the shock tube. Six images are taken after shock impact, and the velocity field at one time is measured using Particle Image Velocimetry (PIV). The images of the density field show the development of a secondary instability in the cylinder. The velocity field provides us with information about the magnitudes of the velocities as well as the magnitude of the vorticity in the flow.

1 Introduction

The interaction of a planar shock with a heavy-gas (SF_6), round cylinder surrounded by air produces strong vorticity, driven by the shock wave's pressure gradient interacting with density gradients at the air/SF_6 interface [1,2]. The passage of the shock across the interface drives the growth of the Richtmyer-Meshkov instability (RMI). The accelerated cylinder becomes highly distorted, producing a column with a crescent-shaped cross section. Vortices rolling up near the tips of the crescent drive the flow of SF_6 into spirals that lead to secondary shear instability and mixing. The growth of the instability is observed using six images of the density profiles of each experimental event, unlike earlier studies, which captured only one image per event. Studies of RMI on quasi-planar interfaces [3–7] have revealed important information about the RMI-driven transition to turbulence, and it now appears that a cylindrical interface is another strong candidate for providing insights into transitional flows. We are also comparing these experimental data to simulations performed using an adaptive mesh Eulerian hydrodynamics code. For more information on this work, see the paper in these proceedings entitled, "Simulations of a shock-accelerated gas cylinder and comparison with experimental results" by C.A. Zoldi, K. Prestridge, P.M. Rightley, R.F. Benjamin, M.L. Gittings, and P. Vorobieff.

2 Experimental Results

The experiment examines a planar slice of a shock-induced flow that is predominantly two-dimensional. The gas shock tube configuration and diagnostics have been described in detail elsewhere [8]. We will briefly summarize the important

features of the experiment here. When the Mach 1.2 normal shock interacts with the heavy gas cylinder, accelerating it to about 100 m/s, baroclinic generation of vorticity causes the RMI [9,10]. Subsequently, secondary shear instability develops.

The cylinder of SF_6 is created by a gravity-feed system. A settling chamber is located above the test section and is filled with SF_6. Glycol droplets that trace the SF_6 [5,11] are inserted into the SF_6 using a theatrical fog generator, which is located inside the settling chamber. An oxygen sensor at the top of the chamber verifies that the amount of oxygen inside the chamber is negligible. A valve is then opened, and gravity drives SF_6 through a tube into the test section. When steady-state flow has been achieved in the test section, as determined through visual inspection, the shock is initiated. The gravity feed system is refilled between every shot to ensure pressure head consistency. The use of the settling tank with the gravity-feed system results in highly reproducible initial conditions.

The post-shock evolution of the cylinder of gas is imaged using a customized, frequency-doubled, Nd:YAG laser sheet to view the glycol particles [11]. Three cameras are mounted around the test section to capture: the initial conditions with a resolution of 55 μm/pixel (IC camera), the dynamic images of the cylinder at 100 μm/pixel resolution (DYN camera), and a double-pulsed PIV image at 16 μm/pixel (PIV camera). The PIV camera has a high enough resolution to resolve the displacements of the glycol droplets using single-frame cross-correlation, corresponding to a velocity vector every 540 μm. As shown in Figure 1, there are seven images from each experiment. After the shock passes, the cylinder rolls into a crescent shape. The tips of the crescent continue to roll inward. At 470 μs, a secondary instability develops in the form of small perturbations on the outer edges of the crescent shape. This instability is highly repeatable from experiment to experiment, and it always appears at the same time in the imaging sequence, with the same wavelength.

Fig. 1. Initial conditions ($t = 0$) and dynamic images ($t = 50, 190, 330, 470, 610, 750\,\mu$s after shock impact) of shock-accelerated gas cylinder

Figure 2a shows the double-pulsed image (the first pulse is the same that illuminates the last dynamic image in Fig. 1) which is interrogated to produce the velocity field shown in Fig. 2b. The mean streamwise velocity of 97 m/s has been subtracted from this field. An outline of the average position of the

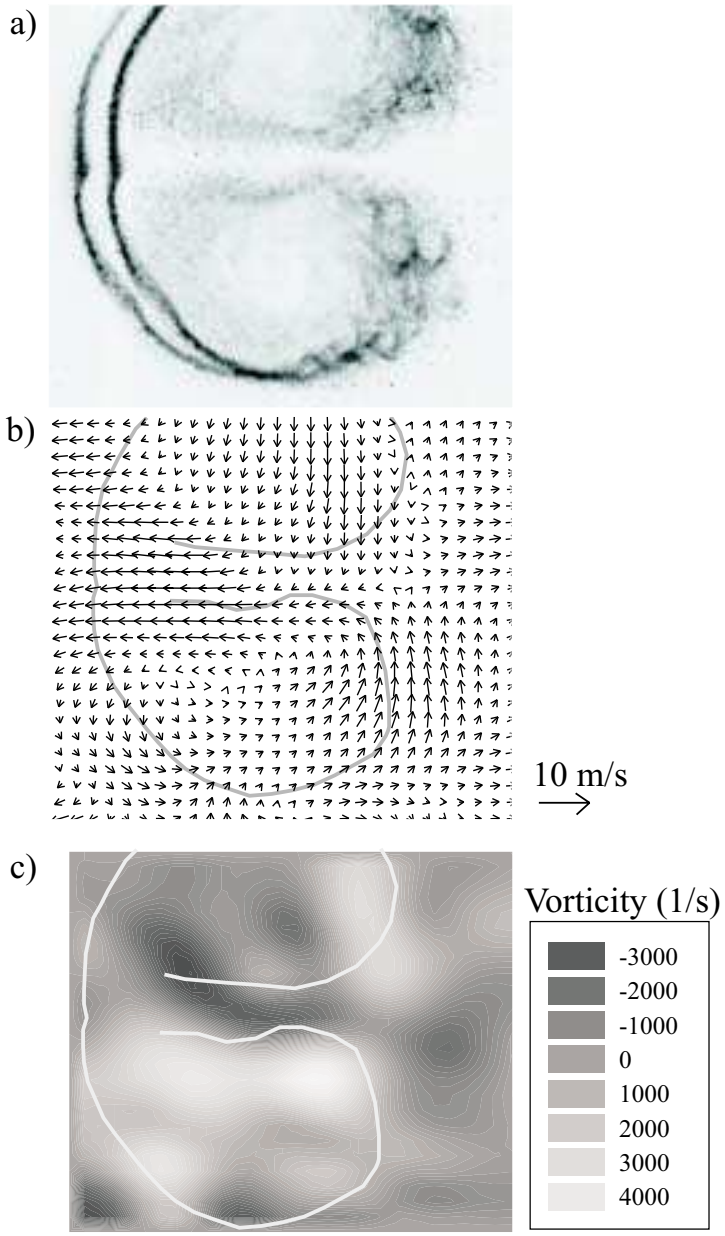

Fig. 2. (**a**)Double-exposed PIV image at $t = 750$ and $762\,\mu$s (Note that the top of the upper vortex is out of the field of view), and (**b**) Corresponding velocity field. (**c**) The corresponding vorticity field. In (**b**) and (**c**), the approximate position of the crescent, midway between the two times, is sketched

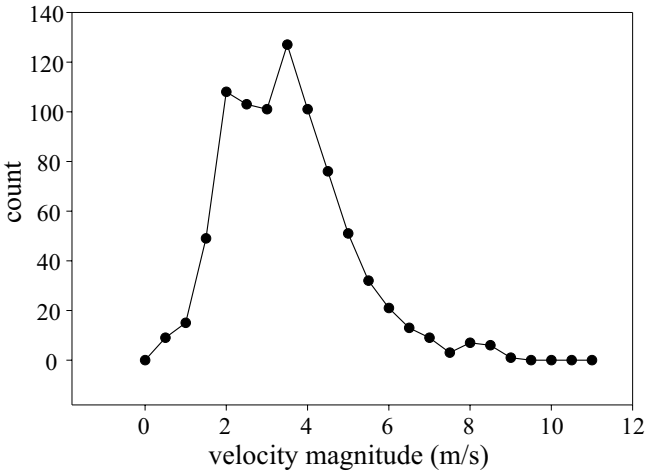

Fig. 3. Histogram of the velocity distribution from Fig. 2(**b**)

cylinder is overlayed on the velocity field to aid in the visualization of the velocity features associated with the counter-rotating vortex pair. The range of velocities observed in the instability flowfield are shown in Fig. 3, a histogram of the velocity distribution from the PIV data. The histogram shows a peak in the velocity magnitude at 4 m/s, and a maximum at 11 m/s. There is a long tail on the distribution, and the bulk of the velocities are between 1 and 7 m/s.

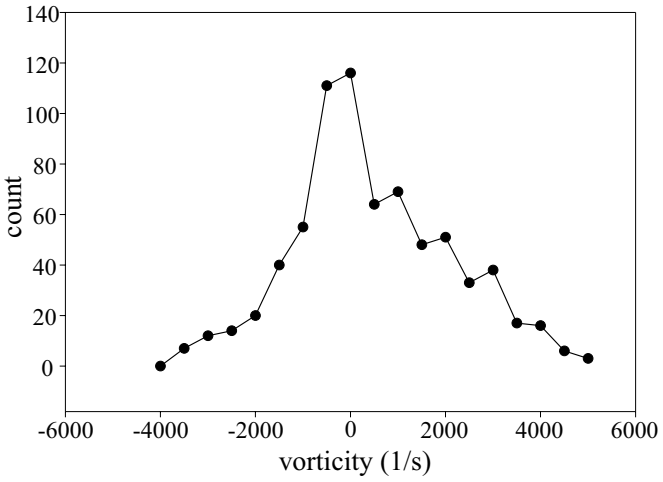

Fig. 4. Histogram of the vorticity distribution from Fig. 2(**c**)

Figure 2c shows the vorticity field associated with the velocity field of Fig. 2b. The two counter-rotating vortices, associated with the curling up of the crescent shape, are visible in the vorticity field. A histogram of the vorticity distribution from the PIV measurement is shown in Fig. 4. This histogram shows a fairly even distribution of vorticity centered around zero. This is expected, since we have two counter-rotating vortices associated with the instability in the cylinder. The peak vorticity magnitude, associated with the vortex cores, is approximately 4000 s^{-1}.

3 Conclusion

We have shown images of the density field and a late-time velocity field of a shock-accelerated fluid instability. The density-field images show the development of two counter-rotating vortices produced by the baroclinic generation of vorticity at the density interface during the passage of the shock wave. They also show the development of a secondary instability along the outer edges of the crescent shape. Particle Image Velocimetry allows us to measure the magnitude of the velocity field at one late time, and from that, we calculate the vorticity field. The peak vorticity associated with the counter-rotating vortices can now be quantified.

Future work in this area includes the study of the instability which develops when two cylinders in close proximity to each other are struck by a shock wave. Preliminary work indicates that there is significant interaction between the cylinders after the passage of the shock wave.

This work was supported by DOE contract W-7405-ENG-36 and by Sandia National Laboratories grant BG-7553.

References

1. J. W. Jacobs (1993). "The dynamics of shock accelerated light and heavy gas cylinders," Phys. Fluids A, **5**(9):2239.
2. J. M. Budzinski (1992). "Planar Rayleigh scattering measurements of shock enhanced mixing," PhD Thesis, California Institute of Technology.
3. J. W. Jacobs, D. G. Jenkins, D. L. Klein, and R. F. Benjamin (1995). "Nonlinear growth of the shock-accelerated instability of a thin fluid layer," J. Fluid Mech., **295**:23.
4. P. Vorobieff, P. M. Rightley, and R. F. Benjamin (1998). "Power law spectra of incipient gas curtain turbulence," Phys. Rev. Lett., **81**(11):2240.
5. P. M. Rightley, P. Vorobieff, and R. F. Benjamin (1999). "Experimental observations of the mixing transition in a shock-accelerated gas curtain," Phys. Fluids, **11**:186.
6. P. Vorobieff, P. M. Rightley, and R. F. Benjamin (1999). "Shock driven gas curtain: fractal dimension evolution in transition to turbulence," Physica D, **133**:469.
7. K. Prestridge, P. Vorobieff, P. M. Rightley, and R. F. Benjamin (2000). "Validation of an instability growth model using particle image velocimetry measurements," Phys. Rev. Lett., **84**(19):4353.

8. K. Prestridge, C. A. Zoldi, P. Vorobieff, P. M. Rightley, and R. F. Benjamin (2001). "Experiments and simulations of instabilities in a shock-accelerated gas cylinder," to appear in Phys. Fluids.
9. R. D. Richtmyer (1960). "Taylor instability in shock acceleration of compressible fluids," Commun. Pure Appl. Math., **23**:297.
10. E. E. Meshkov (1969). "Instability of the interface of two gases accelerated by a shock wave," Izv. Akad. Nauk. SSSR Mekh. Zhidk. Gaza., **4**:151.
11. K. Prestridge, P. M. Rightley, P. Vorobieff, R. F. Benjamin, and N. A. Kurnit (2000). "Simultaneous density-field visualization and PIV of a shock-accelerated gas curtain," Exp. in Fluids, **29**(4):339.